Conformation-specific spectroscopy of alkyl benzyl radicals: Effects of a radical center on the CH stretch infrared spectrum of an alkyl chain

Joseph A. Korn, Daniel P. Tabor, Edwin L. Sibert, and Timothy S. Zwier

Citation: The Journal of Chemical Physics **145**, 124314 (2016); doi: 10.1063/1.4963227
View online: https://doi.org/10.1063/1.4963227
View Table of Contents: http://aip.scitation.org/toc/jcp/145/12
Published by the American Institute of Physics

Conformation-specific spectroscopy of alkyl benzyl radicals: Effects of a radical center on the CH stretch infrared spectrum of an alkyl chain

Joseph A. Korn,[1,a)] Daniel P. Tabor,[2] Edwin L. Sibert III,[2,b)] and Timothy S. Zwier[1,b)]
[1]*Department of Chemistry, Purdue University, West Lafayette, Indiana 47907, USA*
[2]*Department of Chemistry and Theoretical Chemistry Institute, University of Wisconsin, Madison, Wisconsin 53706, USA*

(Received 1 August 2016; accepted 10 September 2016; published online 28 September 2016)

An important initial step in the combustion of gasoline and diesel fuels is the abstraction of hydrogen from alkylbenzenes to form resonance-stabilized alkyl benzyl radicals. This work uses, for the first time, double resonance spectroscopy methods to explore the conformation-specific vibronic and infrared spectroscopy of the α-ethylbenzyl (αEtBz) and α-propylbenzyl (αPrBz) radicals. Local mode Hamiltonian modeling enables assignment of the alkyl CH stretch IR spectra, accounting for Fermi resonance that complicates aliphatic alkyl CH stretch IR spectroscopy. The ground state conformational preferences of the ethyl and propyl chains are changed from those in the alkylbenzenes themselves, with global minima occurring for an in-plane orientation of the alkyl chain (*trans*) about its first dihedral angle (ϕ_{f123}, numbers are alkyl C atoms. C_1 is CH radical site). This in-plane structure is the only observed conformer for the α-EtBz radical, while two conformers, *tt* and *tg′* share this orientation at the first dihedral, but differ in the second (ϕ_{1234}) for the αPrBz radical. The in-plane orientation lowers the local site frequencies of the CH_2 group stretches immediately adjacent to the benzylic radical site by about 50 cm^{-1} relative to those in pure alkyl chains or alkylbenzenes. This effect of the radical site is localized on the first CH_2 group, with little effect on subsequent members of the alkyl chain. In the D_1 excited electronic state, an out-of-plane orientation is preferred for the alkyl chains, leading to torsional mode Franck-Condon activity in the D_0-D_1 spectra that is both conformer-specific and diagnostic of the conformational change. *Published by AIP Publishing.* [http://dx.doi.org/10.1063/1.4963227]

I. INTRODUCTION

Alkylbenzenes make up 10%-30% of the total fuel composition of gasoline and diesel fuels. During combustion, alkylbenzenes follow a complicated set of reaction pathways involving thermal decomposition, oxidation, and under fuel-rich conditions, soot formation. Chemical models of combustion have typically focused attention on simple alkane fuels; however, as major components of transportation fuels, proper modeling of alkylbenzene combustion is crucial to a full understanding of engine performance. Several recent studies have directly studied alkylbenzene combustion.[1–9] Under low-temperature conditions, H-atom abstraction reactions on the alkyl chains (e.g., by OH or OOH) dominate the first steps of combustion. With short alkyl chains ($n \leq 4$), preferential attack occurs at the benzylic site, leading to formation of resonance-stabilized C_6H_5—ĊHR radicals, while longer alkylbenzenes tend to undergo attack elsewhere along the chain by virtue of the larger number of such sites. The preferential formation of resonance-stabilized alkylbenzyl radicals can lead to delayed ignition, a process that has been studied in some detail for n-propylbenzene and n-butylbenzene.[1–3]

Motivated by the central importance of the benzylic radicals formed from n-propylbenzene and n-butylbenzene, we focus attention here on spectroscopic characterization of the α-ethylbenzyl and α-propylbenzyl radicals whose structures are shown below (Scheme 1).

From an electronic standpoint, these radicals are close analogs to the oft-studied benzyl radical,[10–13] whose D_0-D_1 transition occurs in the visible near 454 nm.[10] This transition is weakly allowed, and the electronic origin is therefore weak compared to the set of vibronically induced transitions ~300 cm^{-1} blue of the origin.[11]

More recent studies by Kidwell *et al.* investigated the visible and infrared spectroscopy of α-methyl benzyl radical (αMeBz), which incorporates a methyl rotor directly adjacent to the primary benzylic radical site. The excitation spectrum of αMeBz revealed a stronger origin with Franck-Condon activity built off of it involving the methyl rotor, which changes its preferred orientation and the height of its hindering barrier upon electronic excitation. The alkyl CH stretch infrared spectrum of this radical was also recorded in both the ground (D_0) and first excited (D_1) states. These infrared spectra showed evidence for stretch-bend Fermi resonance, which complicated the analysis and interpretation of those spectra.[14]

Recently, a first-principles local mode Hamiltonian model of the alkyl CH stretch region has been developed and applied to a series of molecules containing alkyl groups.[15–17] The

a)Present address: Department of Chemistry, University of Washington, Seattle, WA 98195 USA.
b)Authors to whom correspondence should be addressed. Electronic addresses: Zwier@purdue.edu and elsibert@wisc.edu

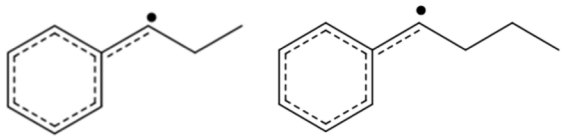

α-ethylbenzyl radical (α-EtBz) α-propylbenzyl radical (α-PrBz)

SCHEME 1.

model, which has produced excellent agreement to date with experiment, includes explicit account of stretch-bend Fermi resonances that are pervasive in the alkyl CH stretch region and hinder the interpretation of such spectra. Development of such a local mode Hamiltonian model paves the way for the alkyl CH stretch region to be used diagnostically on samples containing alkyl groups.[15–17] In particular, the model is now developed to the point that it can play a more predictive role in assessing the conformational preferences of molecules containing alkyl groups via the alkyl CH stretch spectrum.

The present work explores the electronic and alkyl CH stretch infrared spectroscopy of α-ethyl benzyl radical (αEtBz) and α-propyl benzyl radical (αPrBz), the next two members of the series of alkylbenzyl radicals. By increasing in stepwise fashion the length of the alkyl chain attached to the benzylic site, we are afforded an opportunity to explore the effects of this change on the conformational preferences, electronic excited states, and alkyl CH stretch spectra. These longer-chain radicals also offer new tests for developing the first-principles model of the alkyl CH stretch region.

For αEtBz radical, a comparison to the closed shell ethyl benzene molecule can be made.[18] As we shall see, the ethyl group attached to the benzyl radical prefers an in-plane orientation, a preference opposite to that in ethylbenzene, in which the methyl group lies out-of-plane and nearly perpendicular to the plane of the aromatic ring. Extension of the alkyl chain by an additional carbon to form αPrBz radical produces a spectrum with clear evidence for the presence of more than one conformational isomer.

We record conformation-specific infrared and visible spectra using double resonance laser spectroscopy, a first application of these double-resonance tools to free radicals. We find that the conformation-specific vibronic spectra of these radicals show characteristic Franck-Condon activity that reflect the unique changes in geometry of the alkyl chain relative to the benzyl framework upon electronic excitation. A model for the torsional degrees of freedom is developed that is used to fit this activity, playing a significant role in making firm assignments for the conformations responsible for the spectra. The theoretical modeling of the alkyl CH stretch spectra provides a quantitative account of the spectra and adds new insight into the perturbations imposed by the radical site on the alkyl chain. In particular, the CH_2 group immediately adjacent to the benzylic radical site experiences a lowering of its CH site frequency by about 50 cm^{-1}, moving its absorptions to the low-frequency end of the spectrum near 2850 cm^{-1}.

We structure this article as follows. In Sec. II, we describe the experimental and theoretical methods for obtaining spectra. In Sec. III, we present resonant two-photon ionization (R2PI) and ground state resonant ion dip infrared (RIDIR) results for the αEtBz radical, comparing the latter to the model Hamiltonian results. We then turn to R2PI and RIDIR results for the αPrBz radical where the multiple observed conformers, which are revealed by IR-UV holeburning (HB), provide a more complex circumstance. The calculated minimum values of the dihedral angles that describe these conformers vary substantially from one density functional to the next, and the vibrational spectra are sensitive to the calculated values. Nonetheless when both the R2PI and RIDIR spectra are modeled together, clear assignments emerge. Sec. IV provides a summary of the work and highlights the salient findings of this work.

II. METHODS

A. Experimental

The radical precursors, 1-phenylpropanol or R-(+)-1-phenylbutanol (Aldrich), were loaded into the sample compartment of an R. M. Jordan pulsed valve without further purification. The valve was heated to 60-70 °C to obtain a sufficient vapor pressure to seed into high pressure Ar backing gas (1.8 bar). The radical of interest was generated by electric discharge in a short tube fixed to the pulsed valve that contained a pair of discharge electrodes spaced along its channel. The radicals were jet-cooled by expansion into a Wiley-McLaren ion source, as described previously.[14] Two-color resonant two-photon ionization (2C-R2PI) was performed using the scanned visible output of a Nd:YAG pumped dye laser (Narrowscan, Radiant Dyes) as the first, resonant photon. A spatially overlapped, non-resonant UV photon (266.5 nm) generated from the doubled output of a second Nd:YAG pumped dye laser, ionized the molecule. The ions were extracted into a time of flight mass spectrometer, detected by a microchannel plate ion detector, and integrated by a digital oscilloscope to yield the mass resolved 2C-R2PI excitation spectrum.

The ground and excited state vibrational spectra were recorded using resonant ion dip infrared spectroscopy (RIDIRS).[17,19] To obtain the ground state RIDIR spectrum, a 5 Hz tunable, spatially overlapped IR laser (Laservision OPO/OPA) probed the gas pulse ~200 ns prior to the 2C-R2PI process occurring at 10 Hz on a selected transition from the R2PI spectrum belonging to a single conformation of the radical of interest. When the IR laser was resonant with a transition originating from the same ground state as the selected vibronic transition, the ground vibrational state population was depleted, leading to a decrease in ion signal. Using active baseline subtraction through a gated integrator (Stanford Research Systems, SR250), the ground state IR spectrum was obtained for the conformation of the radical being monitored. To obtain the excited state infrared spectrum, the order in time of the resonant visible and tuned IR lasers is exchanged, resulting in an IR-induced depletion of the population in the excited electronic state, again producing a depletion in ion signal. This depletion results from fast non-radiative processes present at the energies above the electronic origin accessed by IR excitation of the excited state radicals.

Conformation-specific vibronic spectra could be obtained using IR-visible holeburning (IR-Vis HB). The method is similar to RIDIRS, but swaps which wavelength is tuned and which is fixed. In this case, a unique IR transition originating from a particular conformer is selected for IR excitation, producing a steady-state depletion of the ground state zero-point level of the conformer of interest. The visible laser is then tuned through the 2C-R2PI spectrum. When the visible laser becomes resonant with a vibronic transition originating from the same ground state as the IR transition, population depletion occurred, with the difference signal (IR on—IR off) producing a conformation-specific vibronic spectrum.

B. Computational

Density functional theory calculation optimizations were carried out using Gaussian09.[20] Conformational minima were verified using relaxed dihedral angle scans about the relevant bonds on the alkyl chain. The αEtBz calculations were performed at the DFT B3LYP/6-311+G(d,p) level of theory, while the αPrBz calculations were performed at the B3LYP/6-31+G(d) level. As an added check on the accuracy and completeness of the conformational search, ground state calculations were performed for αPrBz using M05-2X and ωB97X-D functionals using the 6-31+G(d) basis set, as well as using the B3LYP-D3/aug-cc-pVTZ functional/basis set combination. In order to more fully map out the potential energy surface, conformational scans were obtained along the dihedral angle ϕ_{f123} for select initial values of ϕ_{1234} at the B3LYP/6-311++G(d,p), B3LYP-D3/6-311++G(d,p), and ωB97X-D/6-311++G(d,p) levels of theory. Model spectra at each conformational minimum were obtained using the local mode model Hamiltonian, discussed below.

C. Local mode Hamiltonian model

The model Hamiltonian has been described previously, and the interested reader is referred to recent publications.[17,21,22] In this subsection, we describe a modification to this model that allows us to include torsional effects. As the resulting effects are modest, our description of the Hamiltonian and its matrix elements is brief. We first describe the construction of the Hamiltonian at a given torsional point and then the construction of the torsionally coupled model Hamiltonian using a discrete variable representation (DVR).[23] The potential is evaluated at about ~20 points along the torsional dihedral angle, $\tau = \phi_{f123}$, this being the angle with the lowest barrier to internal rotation. At each point, the remaining coordinates are optimized and the Hessian and linear dipole moments are calculated. To reduce the computational cost of performing the constrained optimizations, all optimizations are performed at the B3LYP/6-311+G(d,p), B3LYP-D3/6-311+G(d,p), and ωB97X-D/6-311+G(d,p) levels of theory. At each torsional point, the model Hamiltonian matrix is constructed following the same procedure as that which is used at the global minimum; the quadratic contribution to the model Hamiltonian is obtained from the Hessian, while the anharmonic terms are assumed to be independent of the dihedral angle. The torsional dependencies of the dipoles and model Hamiltonian matrix elements

$$H_{ij} = \langle i|H_{mod}(\tau)|j\rangle$$

are modeled using a linear least squares fit based on a fourth order expansion of the torsional extension coordinates. For lower barriers, the torsional dependencies would need to be modeled with a Fourier expansion, but for the present results, polynomial expansions yielded good fits.

To solve for the eigenfunctions of the extended Hamiltonian, we treat the torsion using a discrete variable representation.[23] The effective mass, associated with the kinetic contribution of the pure torsional Hamiltonian H_{tor}, is assumed to be constant and corresponds to the appropriate diagonal element of the inverse of the G-matrix.[24] This G^{-1} matrix element is determined, using finite differences, to have a value of 20.1 amu Å^2. The Hamiltonian of the system can thus be written as

$$H = \sum_i \sum_j |i\rangle H_{ij}(\tau) \langle j| + H_{tor} .$$

Both $H_{ij}(\tau)$ and the potential contribution to H_{tor} are evaluated at the DVR torsional points; the kinetic energy contribution to H_{tor} is evaluated using the standard expression of Colbert and Miller.[23] We assume that the overlap matrix between the local vibrational basis functions $|i\rangle$ at different torsional values is the identity matrix, i.e., the states are not dependent on the torsion degree of freedom. In the final comparisons, we scale the torsional potential by a factor of 1.3 to improve agreement between experiment and theory.

III. RESULTS AND ANALYSIS

A. α-ethyl benzyl radical

Before turning to the experimental data, it is useful to summarize the predictions of the calculations regarding the preferred conformations of αEtBz radical in D_0 and D_1 states. The only ground-state conformational minimum for αEtBz found by the calculations places the ethyl side chain in a planar, *trans* configuration, as shown in Figure 1(a). No minimum is found in the excited state at this configuration. Instead, the optimized D_1 structure is calculated to be an out-of-plane *gauche* structure (Figure 1(b)), in which the methyl group carbon is rotated out of plane by 62°. The out-of-plane structure bears some resemblance to the preferred conformation of the closed-shell analog ethylbenzene in both ground and first excited singlet states, in which the methyl group prefers to be out-of-plane.[18]

The 2C-R2PI spectrum of αEtBz is shown in Figure 2. The spectrum displays a strong electronic origin at 21 887 cm^{-1}, with a short, but intense Franck-Condon progression with

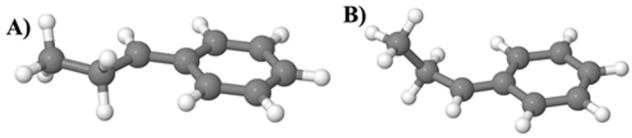

FIG. 1. Structures of α-ethyl benzyl radical calculated at the B3LYP-D3/6-311G++(d,p) level of theory. (a) D_0 optimized, *trans* structure (180°). (b) D_1 optimized *gauche* structure (−118°).

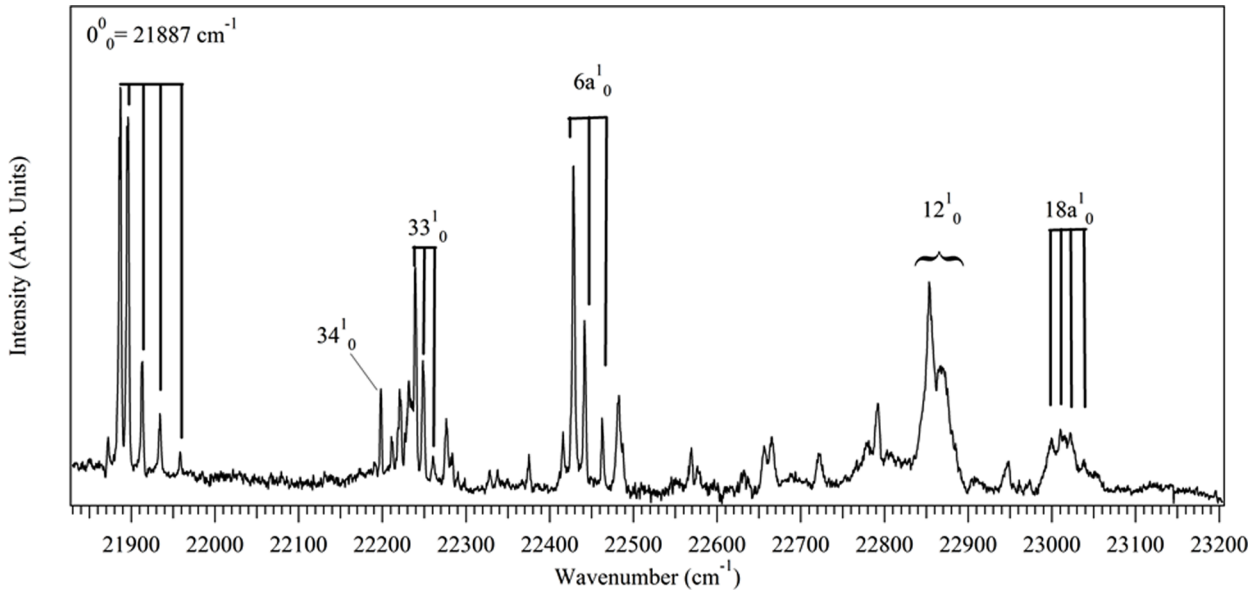

FIG. 2. Two-color R2PI spectrum of αEtBz radical in the D_0-D_1 region.

initial spacing of 9 cm^{-1} and a positive anharmonicity (0-1 = 9 cm^{-1}, 1-2 = 16 cm^{-1}, 2-3 = 21 cm^{-1}, and 3-4 = 24 cm^{-1}). Recalling that αMeBz radical changed the preferred orientation of the methyl group by $\Delta\theta = \pi$,[14] it is not surprising that the ethyl group would undergo a similar reorientation upon electronic excitation, leading to a significant Franck-Condon progression in the torsion of the ethyl group. Indeed, the lowest-frequency vibration of the low-frequency vibration of αEtBz radical in D_0 and D_1 states is calculated to be an out-of-plane wagging of the ethyl group with frequency 28 cm^{-1} and 40 cm^{-1}, respectively, at the B3LYP/6-311++G(d,p) level of theory. We therefore tentatively assign the low frequency progression to the out-of-plane wagging of the ethyl chain, consistent with the calculated change in geometry. We will return shortly to a more quantitative modeling of this Franck-Condon activity.

The transitions 311 and 352 cm^{-1} above the origin in the R2PI spectrum in Figure 2 are tentatively assigned as 34^1_0 and 33^1_0, using Mulliken labelling.[25] Both these vibrations involve in-plane bending modes of the ethyl group. Transitions at 541, 966, and 1109 cm^{-1} are labelled using Varsanyi notation[26] ($6a^1_0$, 12^1_0, and $18a^1_0$) to identify the vibrations common to aromatic derivatives. Their presence here supports the notion that the $\pi\pi^*$ transition of the benzyl moiety leads to similar geometry changes in the ring to those in closed-shell aromatic derivatives. Assignments were made using ground state DFT calculations,[20] by analogy to α-MeBz.[14]

The D_0 RIDIR spectrum of αEtBz is shown at the top of Figure 3. Harmonic frequency calculations fail to capture much of the structure in the spectrum, which experiences significant perturbations from stretch-bend Fermi resonances. The four traces below the experimental spectrum are from the model Hamiltonian, with the full model on top, which reproduces essentially every aspect of the experimental spectrum. The results from the model were calculated at the B3LYP-D3/6-311+G(d,p) level of theory, with the only difference in scaling from our previous work[21] being that the CH_3 stretch frequencies were scaled by 0.9610 instead of 0.9613.[21]

The modeled spectrum in the middle black trace in Figure 3 ("no torsion") is found by diagonalizing the model

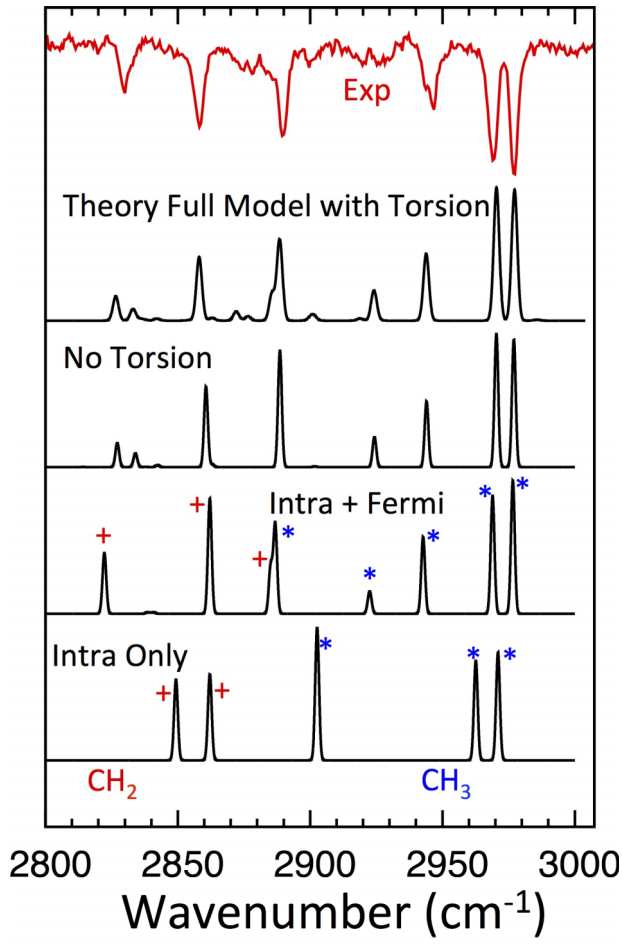

FIG. 3. Ground state RIDIR spectrum (in red) and full model local Hamiltonian model (black, top) for α-EtBz radical, compared with the results with various terms in the model Hamiltonian turned on and off. See text for further discussion. Features marked with a + are related to CH_2 vibrations and * to CH_3 vibrations.

Hamiltonian at the equilibrium geometry of the radical, much as was done in our previous work on alkyl CH stretch spectra.[21] This model captures most of the major features of the spectrum, though there are a few small features in the experiment that are not replicated in the theory. We suspected that these features were due to torsional effects.

To account for these effects, the model Hamiltonian was evaluated at a series of points along a one-dimensional scan of the ϕ_{f123} torsional angle (as described above), with the rest of the coordinates optimized. The torsional coordinate was treated with a discrete variable representation basis,[23] while the remaining elements of the Hamiltonian were fit as a function of the torsion. The G-matrix element associated with the torsion was calculated using finite differences, resulting in an effective moment of inertia of 20.1 amu Å^2.[24] The top black trace in Figure 3 is the result of diagonalizing this augmented Hamiltonian. Inclusion of the torsion results in extra features due to stretch-torsion combination bands, appearing with low intensity at frequencies that match the locations of weak transitions seen in the experimental spectrum.

We can also reduce the complexity of the model Hamiltonian to gain insights into the importance of various coupling terms on the energies and mixing of the states. The trace labeled "Intra + Fermi" in Figure 3 removes the coupling between the CH, CH_2, and CH_3 groups, allowing for specific features to be attributed to individual CH_n groups in the chain. This simplification also results in a reduction of the size of the basis (from 27 to 14), as the combination bands composed of bend fundamentals from more than one group are removed from the basis. However, despite these simplifications, the decoupled Intra + Fermi trace matches the major features of the experiment, showing that the coupling between CH_n groups along the chain does not play a significant role here. This is because the radical center reduces the local mode frequencies of the CH_2 group immediately adjacent to it by about 40 cm^{-1} relative to CH_2 groups in closed shell alkyl chains,[21] giving a site frequency of about 2860 cm^{-1} in α-EtBz, where it is largely decoupled from the CH_3 group. This is evident in the "Intra Only" trace at the bottom of Figure 3, where the features attributed to CH_2 and CH_3 groups are marked with red plus signs and blue asterisks, respectively. When Fermi resonance mixing is included ("Intra + Fermi"), the symmetric stretch modes of both CH_2 and CH_3 groups engage in strong mixing with bend overtones, consistent with expectation.

B. α-propyl benzyl radical (α-PrBz)

The extension of the alkyl chain from ethyl to propyl in α-PrBz radical adds a second dihedral angle that must be specified in characterizing the conformational minima, with the atoms of interest noted on the *tt* conformer in panel (a) of Figure 4. The notation lists the dihedral angles ϕ_{f123} and ϕ_{1234} as *trans* (t, near 180°), perpendicular (p, near 90°), and *gauche* (g or g′ for dihedrals near 60°, either of same or opposite sign to the first dihedral, respectively).

Figure 4(b) locates on a two-dimensional plot the dihedral angles for the optimized conformational minima at the B3LYP-D3/6-311++G(d,p) level of theory. The zero-point corrected relative energies at this level of theory are

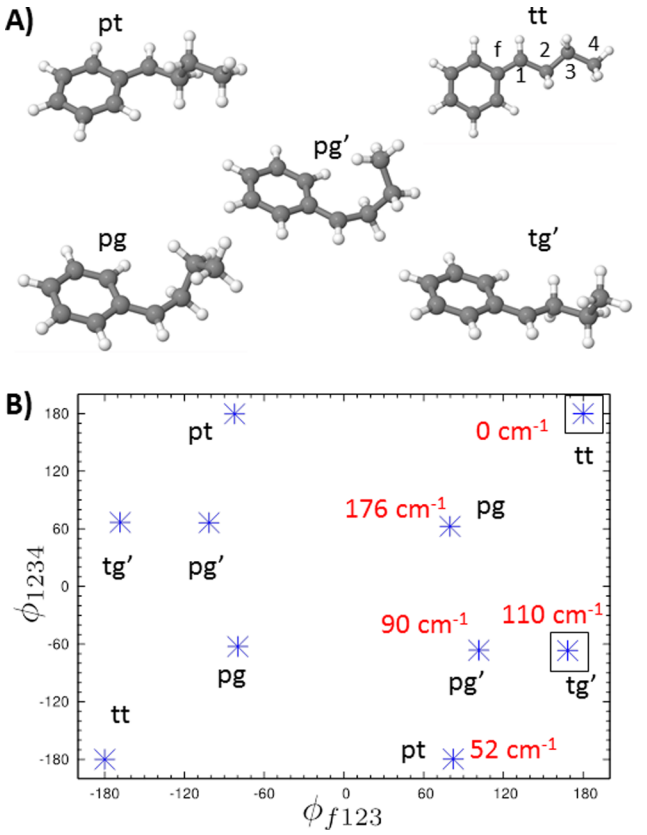

FIG. 4. (a) Structures for the ground state minima of α-propyl benzyl radical at the B3LYP-D3/6-311++G(d,p) level of theory. (b) Two dimensional surface indicating the dihedral angles of the conformational minima. The zero-point corrected relative energies of each conformer are shown in red. There is inversion symmetry about (0, 0). In addition to the *tt* minima at (180, 180) and (−180, −180), there are equivalent minima at (180, −180) and (−180, 180). The black boxes around the *tt* and *tg′* conformers highlight these two conformers as those assigned to conformers A and B, respectively, from experiment.

shown in red. The dihedral angles of these minima can vary substantially depending on the level of theory used. For instance, at the B3LYP-D3/6-311++G(d,p) level, the ϕ_{f123} dihedral angle is 168°. However, when no empirical dispersion correction is employed, the minimum is found to occur at 157°. Differences in computational results for closed-shell alkylbenzyl species were observed previously when employing dispersion correction.[21] The dispersion correction disparity is likely stronger here due to the electronic delocalization extending to the benzyl CH. In addition, there is even disagreement among different levels of electronic theory on which conformers are true minima, most notably with the *pg′* structure, which is a stable minimum at both the ωB97X-D/6-311++G(d,p) and B3LYP-D3/6-311++G(d,p) levels of theory, but is not at B3LYP/6-311++G(d,p). This minimum is only separated from the *tg′* conformer by a low (less than 50 cm^{-1}) barrier for methods that predict its existence. The zero-point corrected relative energetics and ϕ_{f123} and ϕ_{1234} dihedral angles are given in Table I for the three levels of electronic structure theory employed in this work.

The 2C-R2PI spectrum of αPrBz is shown in Figure 5(a), with the D_0-D_1 origin region containing the well-resolved,

TABLE I. Ground state dihedral angles (degrees) and zero-point corrected relative energies (cm^{-1}) of α–PrBz conformers at different levels of electronic structure theory.

	B3LYP[a]			ωB97X-D[a]			B3LYP-D3[a]		
Conformer	ϕ_{f123}	ϕ_{1234}	Energy	ϕ_{f123}	ϕ_{1234}	Energy	ϕ_{f123}	ϕ_{1234}	Energy
tt	180.0	180.0	0.0	180.0	180.0	0.0	180.0	180.0	0.0
pt	98.8	178.0	150.6	81.3	−179.5	43.9	82.2	−179.7	51.8
pg	89.0	63.5	397.0	78.6	61.2	118.7	79.8	62.6	175.8
tg′	157.3	−67.2	207.0	168.0	−66.7	80.3	168.4	−66.7	118.2
pg′	N/A			100.0	−66.1	53.6	101.5	−66.4	90.2

[a]All with the 6-311++G(d,p) basis set.

but congested region between 21 800 and 22 200 cm^{-1} shown in expanded form as the top trace in Figure 5(b). Looking at the unusual intensity pattern of the transitions in this region, it seems likely that more than one conformer is contributing to the spectrum. Notably, the long progression that dominates the appearance of the spectrum in the origin region is far less evident above this region. There also appears to be broadening that begins at about 22 300 cm^{-1}. Using unique IR absorptions identified by the RIDIR spectra (whose discussion follows), two IR-Vis HB spectra were acquired to distinguish the presence and number of conformers present, as well as provide their conformation-specific vibronic spectra. These scans are shown as downward-going traces in black (conformer B) and blue (conformer A) in Figure 5(b).

When the IR holeburn laser was fixed at 2856 cm^{-1}, a set of transitions with D_0-D_1 origin at 21 929 cm^{-1} burned out, ascribed to conformer A (blue trace) in Figure 5(b). An analogous IR-vis holeburn scan with IR laser fixed at 2876 cm^{-1} produced a single-conformer vibronic spectrum due to conformer B (black trace, Figure 5(b)). The latter spectrum displays a long Franck-Condon progression with spacing of ~22 cm^{-1}. It should also be noted that there is an additional weak pair of bands in Figure 7 around 21 700 cm^{-1} that do not burn out in either of the other holeburn scans. This band was weak enough that we could not obtain a RIDIR scan of it. While it seems likely that these transitions belong to a third minor conformer, we have also considered the possibility of a discharge-induced isomerization to the α-Et, α–MeBz radical by studying its spectroscopy. The spectrum of this isomer is different than those shown (see Figure S1 of the supplementary material). The further characterization of the weak bands was not pursued. Attempts to extend the hole-burn scans for conformers A and B into the higher-frequency region

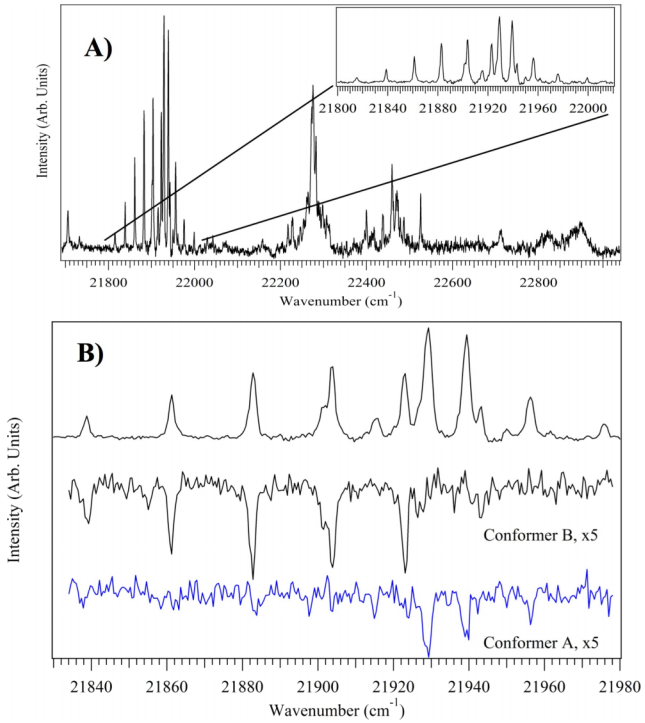

FIG. 5. (a) Overview 2C-R2PI spectrum of α-PrBz radical. (b) Expanded view of the R2PI spectrum over the 21 830-21 980 cm^{-1} region (top) and IR-UV hole-burning spectra recorded with IR hole-burn laser fixed at 2856 and 2876 cm^{-1}, respectively, showing the single-conformer electronic spectra of the two conformers A (blue) and B (black).

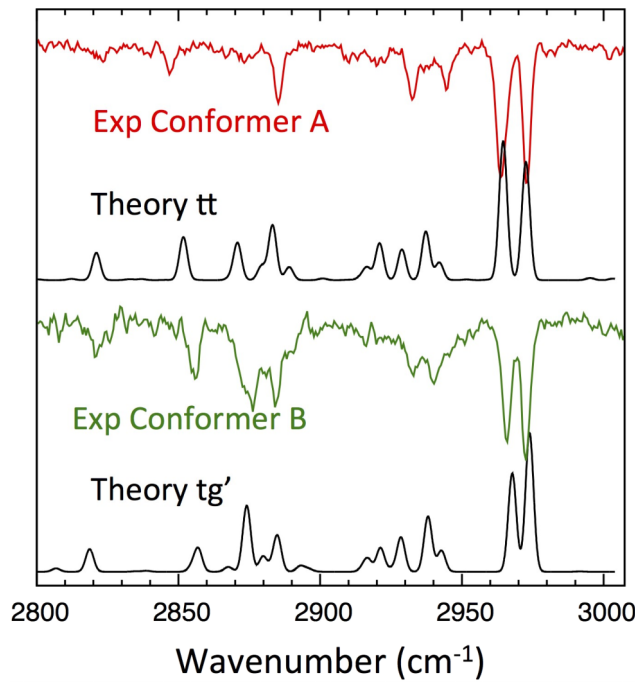

FIG. 6. Experimental and theoretically modeled alkyl CH stretch IR spectra for the two observed conformers of α-PrBz radical. The predictions of the theoretical model for the *tt* and *tg′* conformers are shown, since they are best-fits to the experimental spectra. The theoretical spectra are evaluated at the B3LYP-D3/6-311++G(d,p) level of theory. See text for further discussion.

above 22 000 cm^{-1} were only marginally successful and are not described further.

Figure 6 presents the ground-state RIDIR spectra of conformers A and B over the 2800-3000 cm^{-1} region. The results of application of the full local mode Hamiltonian model for the *tt* and *tg′* conformers of α-PrBz radical are placed directly below the experimental spectra for which they serve as best-fit. These theoretical predictions are based on B3LYP-D3/6-311++(d,p) electronic structure calculations, with more details discussed below. For this radical, we found that the torsion did not make a significant impact on the agreement between the theoretical and experimental spectra. The importance of the torsion decreases in α-PrBz relative to α-EtBz because the moment of inertia of the rotor increases for longer chains (24.6 amu $Å^2$ for the *tt* conformer and 51.0 amu $Å^2$ for the *tg′* conformer).

The results of the model in Figure 6 match experiment reasonably well, but the level of fit is not so high as to leave no doubt as to the assignments based on this fitting alone. This is because the fit is extraordinarily sensitive to the structure of the radical and the level of theory used. As Figure 7 illustrates, the CH_2 local mode frequencies depend critically on the conformation of the chain, particularly the ϕ_{f123} dihedral angle that determines the relative orientation of the CH_2 group on C(2), the carbon atom adjacent to the radical center. The behavior of these frequencies is consistent from one conformer to the next and only depends weakly on the terminal ϕ_{1234} dihedral angle in the α-propyl benzyl radical conformers. Based on a careful inspection of the entire set of conformers of α-PrBz, it is clear that the low frequency transitions in the experimental IR spectra are unique signatures for the presence of a *trans* conformation along the first dihedral angle. No other orientation could contribute such low frequency peaks to the spectrum. It is noteworthy that the *trans* configuration site frequencies at the ωB97X-D/6-311++G(d,p) level of theory for C(2) are systematically shifted about 20 cm^{-1} less than those calculated from the B3LYP/6-311++G(d,p) and B3LYP-D3/6-311++G(d,p) levels of theory. Thus, the model Hamiltonian spectra found using this level of theory have peaks that are systematically shifted upward in the low frequency region.

Though the change in local mode frequencies with respect to the ϕ_{f123} dihedral angle is consistently captured by different levels of electronic structure theory, the location of the minimum geometry for the *tg′* isomer varies substantially from one functional to the next. The methods that include empirical dispersion predict the conformational minimum at a ϕ_{f123} dihedral angle near 168°, whereas the B3LYP/6-311++G(d,p) level of theory without dispersion calculations finds that the minimum has an angle of 157° (Table I). As seen in Figure 7, the CH_2 local mode frequencies change rapidly as a function of the dihedral angle in this region, and therefore, the spectra are quite sensitive to the equilibrium geometry. Spectroscopically, it appears that the B3LYP-D3/6-311++G(d,p) geometry gives the best fit to the experimental spectrum. At the B3LYP/6-311++G(d,p) minimum, the *tg′* theoretical spectrum lacks transitions near 2880 cm^{-1} that are crucial to the assignment.

In order to strengthen these conformational assignments and gain additional insight into the nature of the torsional potential in the D_1 electronic state, we return to the vibronic

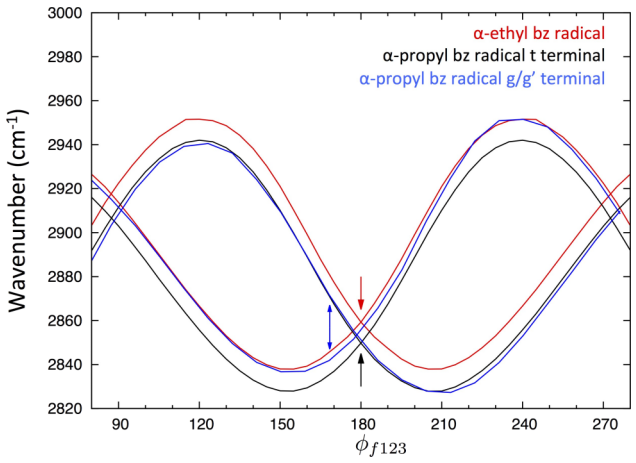

FIG. 7. Local mode frequencies for the CH_2 group immediately adjacent to the benzylic radical site, calculated at the B3LYP-D3/6-311++G(d,p) level of theory, as a function of the dihedral angle for the radicals and conformers of interest. The arrows indicate the dihedral angle at the local minima at the same level of theory.

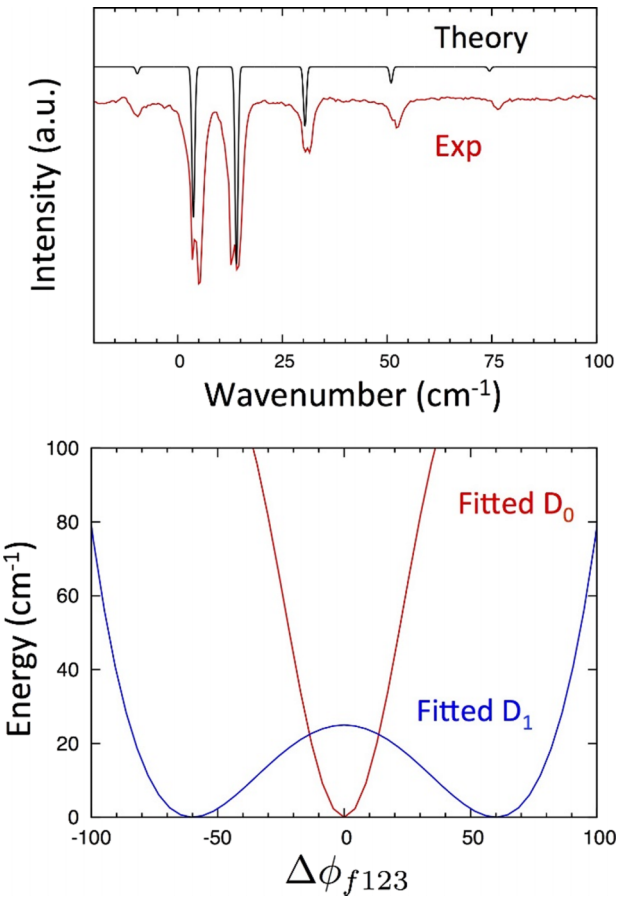

FIG. 8. Top panel: simulated and experimental spectra for the α-EtBz radical. Bottom panel: potential energy surfaces used to calculate the electronic spectra. The surface is fit in terms of $\Delta\phi_{f123}$, where $\Delta\phi_{f123} = \phi_{f123} - \phi_{f123}^{eq}$. The D_1 surface was modeled as a quartic potential with the final parameters $V(\phi_{f123}) = V_0(1 - 2(\Delta\phi_{f123}/\phi_0)^2 + (\Delta\phi_{f123}/\phi_0)^4)$ with $V_0 = 25$ cm^{-1} and $\phi_0 = 60°$. The D_1 surface lies 23 255 cm^{-1} above the ground electronic state at the B3LYP-D3/6-311++G(d,p) level of theory.

spectrum, focusing attention first on the α-EtBz radical (Fig. 8). Upon investigation of the D_1 surface with TD-DFT methods, we found that the electronic surface is a double well with a low barrier at the D_0 electronic state's minimum. The two minima are located near ±120° for each of the three functionals used in the work ($\Delta\phi_{f123}$ = ±60), with a calculated zero-point corrected barrier height between these minima between about 75 and 125 cm^{-1}.

The electronic spectrum shows a Franck-Condon progression with a remarkably low frequency, especially in light of the symmetry of the observed transitions. Given the consistent location of the minima found with different functionals, we only tuned the barrier height when modeling the electronic spectrum. Our goal was to determine if modulating only the barrier height could result in a theoretical spectrum that mimicked the relative intensities and spacing of the experimental spectrum. We found that a small barrier, 25 cm^{-1}, gave a Franck-Condon progression that reproduces experiment remarkably well. This simulation also implies that the true D_0-D_1 origin band is a weak transition ~10 cm^{-1} to the red of the strongest transition in the spectrum. Since the TD-DFT calculations appear to significantly overestimate the barrier on the D_1 surface, such an effect should be anticipated when examining the analogous Franck-Condon activity in the α-PrBz radical. Experimentally, we did not observe evidence for a close-lying D2 state. Additionally, vertical excitation calculations placed the D2 state further above the D1 state energetically than in the case of the benzyl radicals. Further investigation into the D2 electronic effects is not explored in this work, but could warrant investigation.

A similar model was applied to the two conformers of α-PrBz radical, with results shown in Figure 9. Once again, the torsional surface for both the D_0 and D_1 electronic surfaces was parameterized to improve agreement with the experimental spectra. Conformer A of α-PrBz, assigned to the *tt* conformer, exhibits a Franck-Condon profile similar to that in α-EtBz radical. The planar *tt* heavy-atom geometry is a saddle point on the D_1 surface, and its calculated barrier height relative to the out-of-plane minima (located near to $\Delta\phi_{f123}$ = ±70° according to TD-DFT calculations) is found to be between 120 and 150 cm^{-1}.

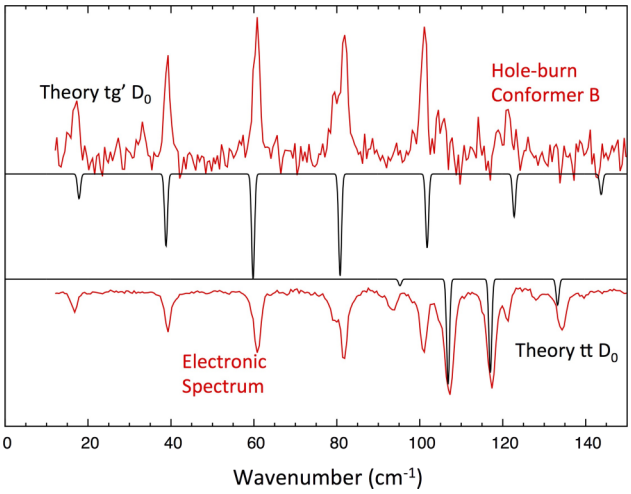

FIG. 9. Comparison of experimental torsional structure of the two conformers of α-PrBz radical with the best-fit results of the theoretical model. See text for further discussion.

It should be noted that the TD-ωB97X-D/6-311++G(d,p) calculations do not identify the *tt* geometry as a saddle point. Instead this geometry is a local minimum lying about 25 cm^{-1} below the out of plane geometry. This appears to be qualitatively incorrect based on the results of the fitting to the electronic spectrum.

The effective moment of inertia of the torsional coordinate used in the modeling must be adjusted due to the longer chain and is calculated to be 24.6 amu $Å^2$. If we retain the same location for the minima (±60°) and the same barrier height (25 cm^{-1}) used in the α-EtBz radical modeling, excellent agreement is obtained between theory and experiment, as shown in Figure 9.

The remaining transitions in the electronic spectra are due to conformer B. We find that this spectrum can also be simulated with some tuning of the parameters of the potential energy surfaces. Here, a much longer Franck-Condon progression is observed. This kind of progression can be simulated by modeling the ground and excited electronic states as displaced harmonic wells, which is the qualitative shape of the two relevant electronic states for the *tg′* conformer. The simulated spectrum depends on two parameters: the frequency of the excited state well and the difference in angle between the minima of the D_0 and D_1 states. For the simulations, we fit the potential of the excited state well to give the correct frequency spacing of ~20 cm^{-1} with a moment of inertia of 53 amu $Å^2$. The effective mass used for the ground state well was 49 amu $Å^2$. As summarized in Table II, the difference between the ground and excited state ϕ_{f123} angles shows an even higher variance across different levels of electronic structure theory than was seen for the ground state minimum geometries. The functionals that include empirical dispersion favor a smaller value for ϕ_{f123} in the D_1 state, giving a difference between angles of at least 55°. By contrast, the B3LYP/6-311++G(d,p) calculations predict that this difference is only about 31°, much closer to the value of 25° that gives the best fit to experiment. When the difference between angles is set to the larger values that are predicted by the empirical dispersion containing functionals, a much longer Frank-Condon progression is seen than is observed in the experiment.

It is worth noting that the experimental Franck-Condon progression shows a rather abrupt cutoff that could be caused by the onset of a non-radiative process that prevents detection of higher vibrational levels in the progression. Indeed, above the origin region, vibronic transitions due to conformer A (e.g., the band at 22 300 cm^{-1} in Figure 5) are clearly evident, but the corresponding long Franck-Condon progressions

TABLE II. D_1 state dihedral angles (degrees) of αPrBz radical conformers at different levels of electronic structure theory.

Level of theory	D_0 tg' ϕ_{f123}	D_1 pg' ϕ_{f123}
B3LYP/6-311++G(d,p)	157.3	126.6
B3LYP-D3/6-311++G(d,p)	168.4	110.2
ωB97X-D/6-311++G(d,p)	168.0	104.2

anticipated for conformer B are notably absent or reduced in intensity.

Finally, we examine the D_1-state IR spectra of the radicals to test the ability of the alkyl CH stretch model to predict spectra accurately in the excited electronic state and to use these spectra to provide an alternative view on the manifestations of the geometry change that occurs upon electronic excitation. Figure 10 shows the experimentally observed and calculated D_1-state IR spectra for α-EtBz radical and the two conformers of α-PrBz radical. We note three aspects of these spectra. First, the experimental D_1-state spectra are quite simple, with fewer transitions carrying significant intensity than their D_0-state counterparts. Second, the pair of transitions at the high frequency end of the spectrum, ascribable in the ground state spectra to the nearly degenerate set of antisymmetric stretch transitions of the methyl group, move around in frequency more than in the ground state. Finally, IR transitions below 2850 cm^{-1} are noticeably missing from the experimental spectra of all three conformers.

In making theoretical predictions for the excited state spectra using the local mode model Hamiltonian, we chose the Hessian parameters for the excited state using the B3LYP/6-311++G(d,p) level of theory, since the parameters that fit the Franck-Condon activity in the electronic spectrum were most closely in line with those predicted by this level of theory, and we anticipate that excited state local mode site frequencies are likely to change rapidly with respect to the ϕ_{f123} angle, as they do in the ground state. The theoretical spectra were evaluated without adjusting the scaling factors or parameters from this level of theory, which were parameterized for the ground electronic state, so the calculated results should only be expected to perform in a qualitative sense. The model's predictive capability is immediately evident from Figure 10, where the major features in the spectrum are reproduced quite well without any adjustment to the model parameters.

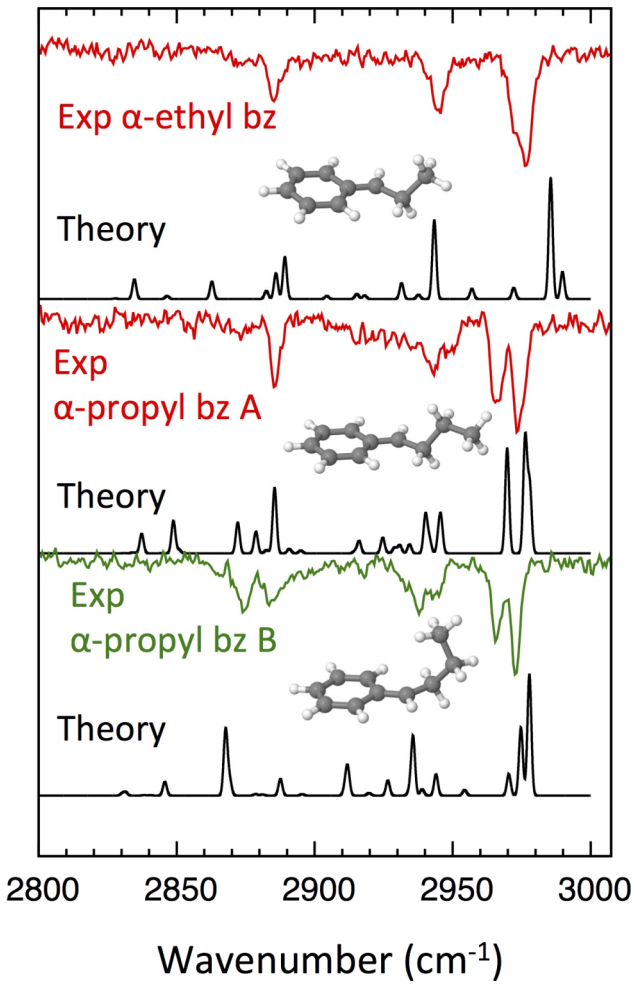

FIG. 10. Excited state IR spectra for α-EtBz and α-PrBz radicals.

Based on the modeling, the fact that none of the spectra show measurable IR absorptions below 2850 cm^{-1} indicates that the CH_2 group adjacent to the radical site in each molecule has changed its orientation upon electronic excitation. In fact, the frequency shifts with changing torsional angle appear to be even more dramatic in the excited electronic state than they are in the ground state. Examining the local mode frequencies of the α-CH_2 group immediately adjacent to the radical site, we find that there is one transition in each of the three radical spectra whose frequency is shifted substantially higher than anything present in the ground state (2976 cm^{-1} for α-ethyl, 2965 cm^{-1} for the *pt* α-propyl, and 2962 cm^{-1} for the *pg′*α-propyl), moving it up into near-overlap with the CH_3 doublet at the high frequency end of the spectrum. This also implies that the angular dependence of the CH_2 local mode frequencies observed on the ground state translates to some degree to the D_1 excited state.

IV. DISCUSSION AND CONCLUSIONS

A. Alkyl chain conformational preferences and their effects on the electronic spectroscopy

A major motivation of the present work is to probe how the conformational preferences of a straight-chain alkyl group attached at the benzylic radical site differ from those in the n-alkylbenzenes, where no such radical site exists. In the n-alkylbenzenes, the first atom in the chain, C(α), is in the plane of the ring, and the first alkyl chain carbon-carbon bond, the C(α)—C(β) bond, prefers an orientation perpendicular to the plane of the aromatic ring. In ethylbenzene, this places the methyl group in this perpendicular configuration, while in propylbenzene, the dihedral angle about the C(α)—C(β) bond is either 180° (*trans*) or ±60° (*gauche*, *g or g′*). While *gauche* defects in pure alkyl chains cost about 3 kJ/mol relative to the unstrained *trans* counterpart, dispersive interactions of the C(γ) group with the aromatic π cloud lower this energy difference to about 1 kJ/mol, so that n-propylbenzene has two conformers, *trans* and *gauche*, which are about equal in population.

These preferences are completely changed in the first two members of the α-alkyl benzyl radical series studied here, α-EtBz and α-PrBz radical. In α-EtBz radical, the ethyl chain prefers an in-plane orientation (*trans*), with no minimum found at the levels of theory explored here at the perpendicular geometry. In α-PrBz radical, this preference for an all in-plane geometry continues, with the *tt* structure the global minimum (Figure 4). The other observed conformation, *tg′*, is

calculated to be 110 cm^{-1} up in energy at the B3LYP-D3/6-311++G(d,p) level of theory. While this energy separation is smaller than that anticipated for a single gauche defect in a pure alkane, what is perhaps more striking is that the calculation also predicts several minima (*pt*, *pg′*, *pg*) with very low energies that are (nearly) perpendicular geometry about the ϕ_{f123} dihedral (Figure 4). While the experimental absence of such structures likely points to an incorrect ordering of the calculated energies of these minima relative to *tt* and *tg′*, it is clear that the longer alkyl chains take up a wider range of geometries that suggest that the radical site presents a softer potential for re-orientation of the alkyl chain.

Upon $\pi\pi^*$ electronic excitation, the preference for an in-plane geometry about the ϕ_{f123} dihedral is lost. Calculations predict at best a shallow in-plane minimum with a preferred geometry more nearly *gauche* about the first dihedral. This leads to the strong Franck-Condon activity observed in the low-frequency torsion associated with this dihedral, which we have successfully modeled.

B. The effect of the radical site on the alkyl CH stretch spectra

A second motivation for this work was to explore the opportunity the alkylbenzyl radicals present for obtaining single-conformer IR spectra in the alkyl CH stretch region, in the hopes that such data could be used to understand the effects of the benzylic radical site on the alkyl CH stretch IR spectroscopy. Given the pervasive presence of stretch-bend Fermi resonances, fitting these spectra required a model that treated such effects explicitly and accurately. To that end, the local mode model Hamiltonian approach we have developed for alkyl chains of stable molecules was applied here to the alkylbenzyl radicals. A defining strength of the local mode approach is that it enables extraction of local site frequencies and inter-bond and stretch-bend couplings along the chain.

Several key deductions grew out of the first-principles modeling on α-EtBz and α-PrBz radicals. First, the local mode frequencies of the CH_2 group next to the radical site are very sensitive to the dihedral angle and therefore are diagnostic of that dihedral. The CH_2 site frequencies drop down to around 2850 cm^{-1} near the in-plane (*trans*) configuration, and this allows us to clearly establish that all three observed conformers are *trans* about the first dihedral angle. We surmise on this basis that the hyperconjugation of the out-of-plane CH bonds of this first CH_2 group with the π orbital of the benzylic radical site lowers this frequency by about 50 cm^{-1} relative to alkyl chain CH_2 groups in other contexts.

Second, this lowering of the CH_2 local site frequencies adjacent to the radical center has the effect of spreading the IR spectrum of α-EtBz radical into separate regions due to the CH_2 and CH_3 groups, as seen in Figure 3. Unlike in the closed shell case, there are no multiple symmetric stretch fundamentals in the same frequency region. Because of this, the CH_2 and CH_3 groups are essentially decoupled from one another, simplifying the modeling in α-EtBz radical by eliminating the need for dipole decomposition in modeling the IR intensities. The results of the model capture the experimental spectrum with quantitative accuracy.

Third, this firm foundation of successful fitting of the ground state IR spectrum served as the basis for a more-or-less complete treatment of all aspects of the IR and vibronic spectroscopy of α-EtBz radical, including the effects of torsional degrees of freedom in both ground and excited states. The pleasing result is that the IR and vibronic spectroscopy reports on the ethyl group torsion in the two electronic states in complementary and consistent ways.

For the α-PrBz radical, the assignment process was complicated by the potential presence of several conformational isomers. Experimentally, IR-UV holeburning was applied for the first time to spectra of free radicals to separate successfully the R2PI spectrum into its single-conformer components. Based on our modeling of the alkyl CH stretch spectra, it was possible to eliminate certain structures as candidates, but the predicted spectra were not sufficiently diagnostic or accurate to make firm assignments on that basis alone. Firm assignments came only after successful modeling of the Franck-Condon activity present in the vibronic spectrum. By applying the same method successfully developed for α-EtBz, we are able to characterize the torsional FC activity of conformer A and assign it firmly as the *tt* conformer. The long FC progression present in conformer B was then modeled via displaced harmonic wells, leading to its assignment to the *tg′* conformer, with a difference in the equilibrium dihedral angles (25°) near that predicted by calculations using the DFT B3LYP functional.

Finally, we obtained conformer-specific IR spectra in the excited electronic state for these radicals using a three-laser scheme in which the IR laser used to deplete the D_1 origin was inserted between the two UV laser pulses used in the 2C-R2PI process. The set of three D_1-state alkyl CH stretch IR spectra were modeled with minimal modification relative to its ground-state counterpart. The disappearance of low frequency IR features observed experimentally is consistent with the change in preference for the ϕ_{f123} torsional angle from in-plane to out-of-plane upon electronic excitation, demonstrating that the geometry change deduced from the vibronic spectrum also has clear spectral consequences in the alkyl CH stretch IR spectrum.

SUPPLEMENTARY MATERIAL

See supplementary material for the vibronic spectrum of α-methyl-α-ethyl benzyl radical.

ACKNOWLEDGMENTS

J.A.K. and T.S.Z. gratefully acknowledge support for this research from the Department of Energy, Basic Energy Research, Chemical Sciences Division under Grant No. DE-FG02-96ER14656. D.P.T. and E.L.S. acknowledge support from the NSF via Grant No. CHE-1213449.

[1]D. Darcy, M. Mehl, J. M. Simmie, J. Würmel, W. K. Metcalfe, C. K. Westbrook, W. J. Pitz, and H. J. Curran, Proc. Combust. Inst. **34**, 411–418 (2013).

[2]D. Darcy, H. Nakamura, C. J. Tobin, M. Mehl, W. K. Metcalfe, W. J. Pitz, C. K. Westbrook, and H. J. Curran, Combust. Flame **161**, 65–74 (2014).

[3]D. Darcy, C. J. Tobin, K. Yasunaga, J. M. Simmie, J. Würmel, W. K. Metcalfe, T. Niass, S. S. Ahmed, C. K. Westbrook, and H. J. Curran, Combust. Flame **159**, 2219–2232 (2012).
[4]H. Nakamura, D. Darcy, M. Mehl, C. J. Tobin, W. K. Metcalfe, W. J. Pitz, C. K. Westbrook, and H. J. Curran, Combust. Flame **161**, 49–64 (2014).
[5]M. Mehl, O. Herbinet, P. Dirrenberger, R. Bounaceur, P.-A. Glaude, F. Battin-Leclerc, and W. J. Pitz, Proc. Combust. Inst. **35**, 341–348 (2015).
[6]V. S. F. Muralha, R. M. Borges dos Santos, and J. A. Martinho Simões, J. Phys. Chem. A **108**, 936–942 (2004).
[7]F. Battin-Leclerc, V. Warth, R. Bounaceur, B. Husson, O. Herbinet, and P.-A. Glaude, Proc. Combust. Inst. **35**, 349–356 (2015).
[8]O. Herbinet, B. Husson, M. Ferrari, P.-A. Glaude, and F. Battin-Leclerc, Proc. Combust. Inst. **34**, 297–305 (2013).
[9]O. Herbinet, B. Husson, H. Le Gall, and F. Battin-Leclerc, Chem. Eng. Sci. **131**, 49–62 (2015).
[10]M. Fukushima and K. Obi, J. Chem. Phys. **93**, 8488–8497 (1990).
[11]M. Fukushima and K. Obi, J. Chem. Phys. **96**, 4224–4232 (1992).
[12]M. Heaven, L. Dimauro, and T. A. Miller, Chem. Phys. Lett. **95**, 347–351 (1983).
[13]H. S. Im and E. R. Bernstein, J. Chem. Phys. **95**, 6326 (1991).
[14]N. M. Kidwell, N. J. Reilly, B. Nebgen, D. N. Mehta-Hurt, R. D. Hoehn, D. L. Kokkin, M. C. McCarthy, L. V. Slipchenko, and T. S. Zwier, J. Phys. Chem. A **117**, 13465–13480 (2013).
[15]E. G. Buchanan, J. C. Dean, T. S. Zwier, and E. L. Sibert, J. Chem. Phys. **138**, 064308 (2013).
[16]E. G. Buchanan, E. L. Sibert, and T. S. Zwier, J. Phys. Chem. A **117**, 2800–2811 (2013).
[17]E. L. Sibert, D. P. Tabor, N. M. Kidwell, J. C. Dean, and T. S. Zwier, J. Phys. Chem. A **118**, 11272–11281 (2014).
[18]D. R. Borst, P. W. Joireman, D. W. Pratt, E. G. Robertson, and J. P. Simons, J. Chem. Phys. **116**, 7057–7064 (2002).
[19]T. S. Zwier, J. Phys. Chem. A **105**, 8827–8839 (2001).
[20]G. W. T. M. J. Frisch, H. B. Schlegel, G. E. Scuseria, J. R. C. M. A. Robb, G. Scalmani, V. Barone, B. Mennucci, H. N. G. A. Petersson, M. Caricato, X. Li, H. P. Hratchian, J. B. A. F. Izmaylov, G. Zheng, J. L. Sonnenberg, M. Hada, K. T. M. Ehara, R. Fukuda, J. Hasegawa, M. Ishida, T. Nakajima, O. K. Y. Honda, H. Nakai, T. Vreven, J. A. Montgomery, Jr., F. O. J. E. Peralta, M. Bearpark, J. J. Heyd, E. Brothers, V. N. S. K. N. Kudin, T. Keith, R. Kobayashi, J. Normand, A. R. K. Raghavachari, J. C. Burant, S. S. Iyengar, J. Tomasi, N. R. M. Cossi, J. M. Millam, M. Klene, J. E. Knox, J. B. Cross, C. A. V. Bakken, J. Jaramillo, R. Gomperts, R. E. Stratmann, A. J. A. O. Yazyev, R. Cammi, C. Pomelli, J. W. Ochterski, K. M. R. L. Martin, V. G. Zakrzewski, G. A. Voth, J. J. D. P. Salvador, S. Dapprich, A. D. Daniels, J. B. F. O. Farkas, J. V. Ortiz, J. Cioslowski, and D. J. Fox, GAUSSIAN 09, Revision D.01, Gaussian, Inc., Wallingford CT, 2010.
[21]D. P. Tabor, D. M. Hewett, S. Bocklitz, J. A. Korn, A. J. Tomaine, A. K. Ghosh, T. S. Zwier, and E. L. Sibert, J. Chem. Phys. **144**, 224310 (2016).
[22]E. L. Sibert, N. M. Kidwell, and T. S. Zwier, J. Phys. Chem. B **118**, 8236–8245 (2014).
[23]D. T. Colbert and W. H. Miller, J. Chem. Phys. **96**, 1982–1991 (1992).
[24]J. C. D. E. B. Wilson and P. C. Cross, *Molecular Vibrations* (Dover, New, York, 1955).
[25]R. Mulliken, J. Chem. Phys. **23**, 1997–2011 (1955).
[26]G. Varsanyi, *Assignments for Vibrational Spectra of 700 Benzene Derivatives* (Wiley, New York, 1974).